Predicting the flow induced fibre orientation of highly concentrated suspensions using a micro-macro modelling

P. Dumont, S. Le Corre, L. Orgéas, D. Favier

Laboratoire Sols – Solides – Structures,
C.N.R.S. – Université Joseph Fourier – Institut National Polytechnique de Grenoble,
BP53, 38041 Grenoble cedex 9, FRANCE
URL: www.3S.hmg.inpg.fr *e-mail: Pierre.Dumont@hmg.inpg.fr; Steven.Lecorre@hmg.inpg.fr*
e-mail: Laurent.Orgeas@hmg.inpg.fr;Denis.Favier@hmg.inpg.fr

ABSTRACT: An upscaling model has been developed to analyse the rheology of highly concentrated planar fibre suspensions. Fibres are in plane oriented rigid cylinders with elliptical cross section. Fibre-fibre interactions at their contacting points are Newtonian. Some "numerical rheological experiments" are achieved on representative fibre networks in order to analyse the evolution of the orientation of the whole fibres as functions of the macroscopic strain rate, the initial orientation and fibre content.

Key words: fibre suspension, micro-macro modelling, rheology, fibre orientation

1 INTRODUCTION

The rheology of fibre suspensions is strongly affected by the spatial orientation, the connexion and the distribution of fibres. Among the numerous studies devoted to this complex problem, few focused on highly concentrated suspensions [1]. In that case, a commonly admitted assumption [2-4] consists in neglecting the influence of the liquid matrix on the overall behaviour of the suspension, its rheology being mainly induced by fibre-fibre interactions. Accounting for such an hypothesis, the paper is addressing the modelling of the rheology of highly concentrated suspensions using a micro-macro approach based on the theory of homogenisation of discrete media [5-6]. Within this framework, we consider a 2D suspension made by a network of connected rigid fibres. The mechanical fibre-fibre interaction is associated with the shearing of a small amount of Newtonian liquid matrix entrapped between the fibres.
In previous works [7-9], theoretical results gave the nature of the macroscopic equivalent continuous medium of this kind of discrete networks. Moreover, to study more precisely the rheology of the equivalent medium, fibre networks were generated, allowing to obtain isotropic as well as oriented microstructures. "Numerical mechanical experiments", *i.e.* homogeneous macroscopic deformation at given strain rate, were performed using these microstructures. These experiments allowed to determine the stress – strain rate relations.
In the present paper, similar tests were achieved in order to analyse the evolution of the orientation of the whole fibres as functions of the macroscopic strain rate, the initial orientation and fibre content.

2 MICROSTRUCTURES

In this work (see fig. 1), the fibre network forming the suspension is made by an assembly of in-plane oriented ($\underline{\mathbf{e}}_1$, $\underline{\mathbf{e}}_2$), rigid and identical cylinders (length l, elliptical cross-section with minor axis d_{min} and major axis $d_{max} << l$, the major axis belonging to ($\underline{\mathbf{e}}_1$, $\underline{\mathbf{e}}_2$)).

Each fibre has multiple mechanical contact points with the neighbouring fibres. During the deformation of the network, the Newtonian liquid entrapped around each contact point is sheared due to the relative motion between fibres, leading to viscous interaction forces and moments. In the case slender fibres ($d_{max} << l$), it was shown previously

that the influence of moments on the deformation of the fibre network could be neglected compared to the influence of forces [7-9], whose expression at a contact point Q is:

$$\underline{\mathbf{f}}^{c/b} = -\frac{\eta_0 \, d_{\max}^{\,2}}{h \sin\varphi} \left(\underline{\mathbf{v}}^b(Q) - \underline{\mathbf{v}}^c(Q) \right) \qquad (1)$$

where $\underline{\mathbf{v}}^b(Q)$ and $\underline{\mathbf{v}}^c(Q)$ are the velocities of point Q belonging to the fibres b and c, respectively, η_0 the Newtonian viscosity of the matrix, h the thickness of the contact zone, φ the angle between the two fibres (see fig.1).

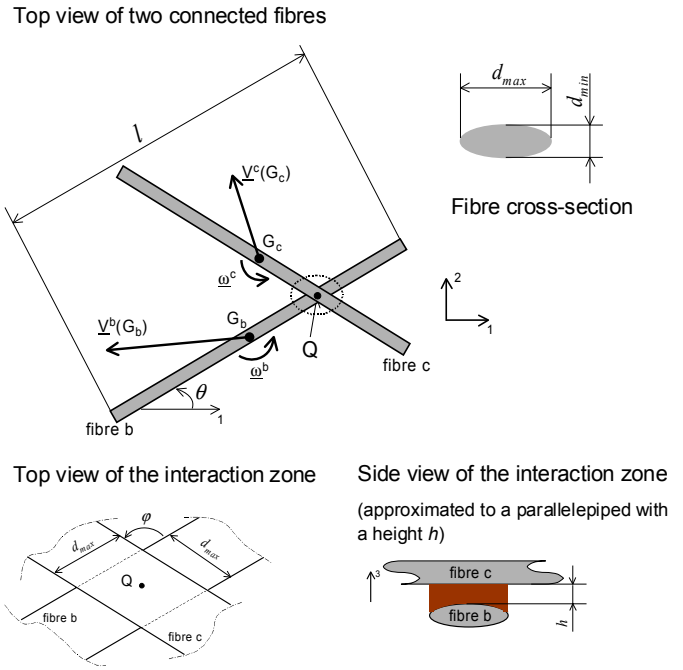

Fig.1: definition of the fibre geometry and the fibre-fibre interaction.

In order to generate representative fibre networks, the methodology described hereafter was adopted:

1. A thin box with dimensions $l_0 \times l_0 \times t$, ($t << l_0$) was first considered, the square cross-section $l_0 \times l_0$ belonging to the plane of the network ($\underline{\mathbf{e}}_1$, $\underline{\mathbf{e}}_2$).
2. Given the fibre geometry and volume fraction $f^{(f)}$, calculate the number N of fibres contained in the volume of the cell.
3. Equi-distribute the in-plane coordinates x_{Gi1} and x_{Gi2} of the centres of mass G_i of each fibre.
4. Calculate the in-plane angles of orientation θ_i of the fibres i. In the case of isotropic networks, these angles are uniformly distributed in the range $]-\pi/2, \pi/2]$. If the network is orientated, values of angle follow a Gaussian distribution function. In this work, all the generated networks have a mean orientation θ of 0 or $\pi/2$.
5. Give vertical positions x_{Gi3} of the centres of mass G_i of the fibres. Determine the contact points between fibres using geometrical considerations [10]: a contact point exists if the gap between neighbouring fibres is smaller than a specified value (in a similar strategy as in [11-12]).

Fig. 2 depicts two microstructures obtained by this generation process, one for an isotropic cell A and one for an orientated network B. The second order orientation tensor $\underline{\underline{\mathbf{a}}}$ was used as a macroscopic measure of the fibre network orientation:

$$\underline{\underline{\mathbf{a}}} = \frac{1}{N} \sum_{k=1}^{N} \underline{\mathbf{p}}_k \otimes \underline{\mathbf{p}}_k \qquad (2)$$

where $\underline{\mathbf{p}}_k$ is the unit fibre orientation vector of fibre k. The approximation ψ_a of the orientation distribution function ψ was also calculated in terms of the orientation tensor as follows [1]:

$$\psi_a(\theta) = \frac{1}{\pi} + \frac{4}{\pi} \left(\underline{\underline{\mathbf{a}}} - \frac{1}{2} \underline{\underline{\boldsymbol{\delta}}} \right) : \left(\underline{\mathbf{p}} \otimes \underline{\mathbf{p}} - \frac{1}{2} \underline{\underline{\boldsymbol{\delta}}} \right) \qquad (3)$$

where $\underline{\mathbf{p}} = \cos\theta \, \underline{\mathbf{e}}_1 + \sin\theta \, \underline{\mathbf{e}}_2$ and where $\underline{\underline{\boldsymbol{\delta}}}$ is the identity tensor. With the generation process adopted in this work, fig. 2 shows that such kind of simple macroscopic measure leads to a rather good approximation ψ_a of the orientation distribution function ψ

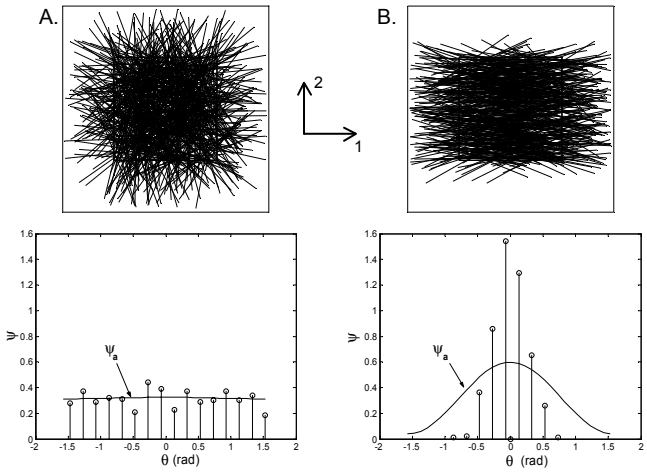

Fig. 2: representative elementary fibre networks generated with $l_0 = 25$ mm, $t = 2.5$ mm, $l = 25$ mm, $d_{\min} = 0.06$ mm, $d_{\max} = 0.68$ mm, $f^{(f)} = 0.25$, $N = 484$. A – Isotropic network ($a_{11} = a_{22} = 0.5$, $a_{12} = 0$). B – Orientated network ($a_{11} = 0.9$, $a_{22} = 0.1$, $a_{12} = 0$)

3 MICRO-MACRO MODELLING

To obtain the equivalent macroscopic rheological behaviour of such fibre networks, the homogenisation of discrete structures was used [7-9]. Under the assumptions of periodicity and scale separation (the size of the whole suspension L is supposed to be much greater than the size of the microstructure period l_0), it was established that the equivalent macroscopic medium was an usual Cauchy medium whose macroscopic momentum balance is:

$$\underline{\underline{\mathbf{div}}}\ \underline{\underline{\boldsymbol{\sigma}}} = \underline{\mathbf{0}} \tag{4}$$

where $\underline{\underline{\boldsymbol{\sigma}}}$ is the macroscopic stress tensor, found to be a linear anisotropic function of the macroscopic strain rate tensor $\underline{\underline{\mathbf{D}}}$.

4 EVOLUTION OF THE FIBRE ORIENTATION

The stress – strain rate relation was analysed quantitatively in previous works, by studying numerically the mechanical response of given representative elementary fibre networks to imposed strain rates [7-9]. A similar approach is adopted here to study the rate of the second order orientation tensor :

$$\dot{\underline{\underline{\mathbf{a}}}} = \frac{1}{N}\sum_{k=1}^{N} \left(\dot{\underline{\mathbf{p}}}_k \otimes \underline{\mathbf{p}}_k + \underline{\mathbf{p}}_k \otimes \dot{\underline{\mathbf{p}}}_k \right) \tag{5}$$

as a function of the imposed strain rate, the current orientation $\underline{\underline{\mathbf{a}}}$ and the fibre content $f^{(f)}$.
For that purpose, representative elementary fibre networks similar to those displayed in fig. 2 were submitted to a macroscopic elementary and irrotational strain rate $\underline{\underline{\mathbf{D}}} = \lambda\, \underline{\underline{\mathbf{D}}}_1 = \lambda\, \underline{\mathbf{e}}_1 \otimes \underline{\mathbf{e}}_1$, λ being a real scalar (see fig. 3 for the corresponding transformation):

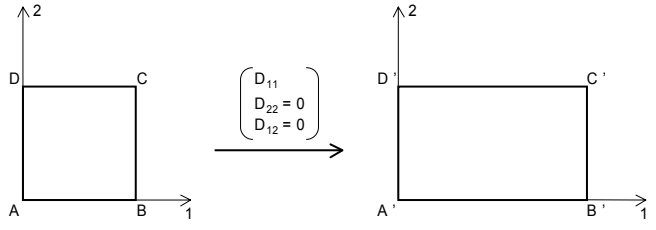

Fig. 3: kinematics used to deform the fibre networks

4.1 *Influence of the strain rate*

Given the current fibre orientation $\underline{\underline{\mathbf{a}}}$ and volume fraction $f^{(f)}$, theoretical results proved that $\dot{\underline{\underline{\mathbf{a}}}}$ is a linear function of the imposed macroscopic strain rate $\underline{\underline{\mathbf{D}}}$:

$$\dot{\underline{\underline{\mathbf{a}}}}\,(\lambda\, \underline{\underline{\mathbf{D}}}_1) = \lambda\, \dot{\underline{\underline{\mathbf{a}}}}\,(\underline{\underline{\mathbf{D}}}_1) \tag{6}$$

This is illustrated by numerical simulation in fig. 4 where the components $\dot{a}_{ij}$ of $\dot{\underline{\underline{\mathbf{a}}}}$ in ($\underline{\mathbf{e}}_1$, $\underline{\mathbf{e}}_2$) have been plotted as functions of λ.

Please also note that for the imposed macroscopic strain rate, $\dot{a}_{12}$ plotted in fig. 4 equals zero: principal axes of orientation remain the same.

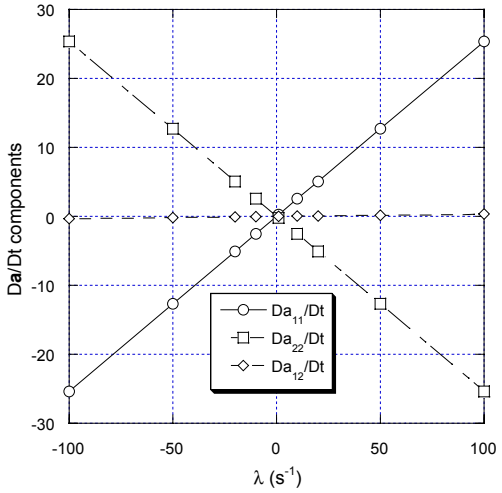

Fig. 4: Influence of the strain rate on the components $\dot{a}_{ij}$ of $\dot{\underline{\underline{\mathbf{a}}}}$ in ($\underline{\mathbf{e}}_1$, $\underline{\mathbf{e}}_2$) – $f^{(f)} = 0.25$, $a_{11} = 0.7$, $a_{22} = 0.3$, $a_{12} = 0$

4.2 *Influence of the fibre orientation*

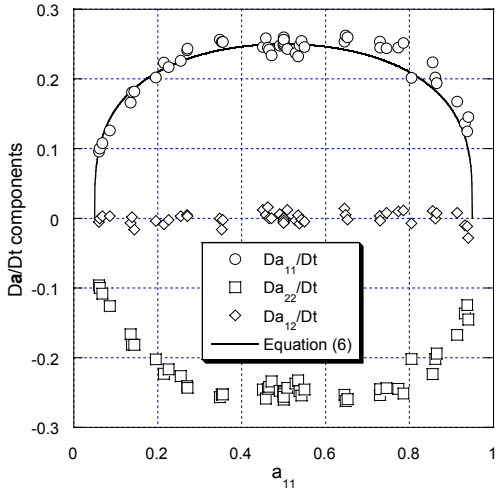

Fig. 5: Influence of the current orientation a_{11} (a_{22} = 1-a_{11}, $a_{12} = 0$) on the components $\dot{a}_{ij}$ of $\dot{\underline{\underline{\mathbf{a}}}}$ – $f^{(f)} = 0.25$, $\lambda = 1\ s^{-1}$.

Fig. 5 shows the evolution of the components of $\dot{\underline{\underline{\mathbf{a}}}}$ (in ($\underline{\mathbf{e}}_1$, $\underline{\mathbf{e}}_2$)) as a function of the current orientation $\underline{\underline{\mathbf{a}}}$

at given strain rate and fibre volume fraction. Such a figure underlines the strong influence of $\underline{\underline{\mathbf{a}}}$ on $\dot{\underline{\underline{\mathbf{a}}}}$. Whatever the current orientation, fibres tends to align in the elongation direction.

4.3 Influence of the fibre volume fraction

The influence of the current fibre volume fraction $f^{(f)}$ was also analysed at given strain rate and fibre orientation. This is illustrated in fig. 6, which reveals a very slight influence of $f^{(f)}$ on $\dot{\underline{\underline{\mathbf{a}}}}$, at least in the investigated range.

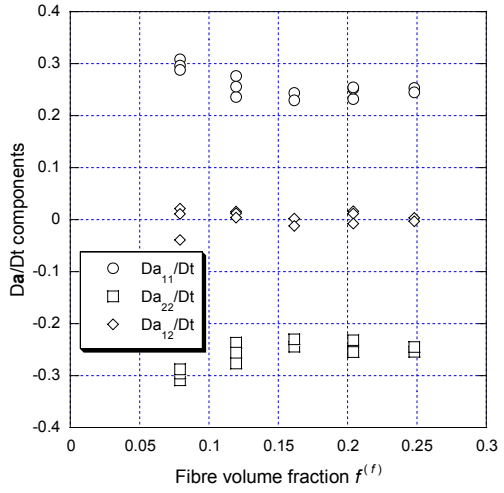

Fig. 6: Influence of the current fibre volume fraction on the components $\dot{a}_{ij}$ of $\dot{\underline{\underline{\mathbf{a}}}}$ – $a_{11} = 0.7$, $a_{22} = 0.3$, $a_{12} = 0$, $\lambda = 1$ s^{-1}

4.4 Time evolution of the fibre orientation

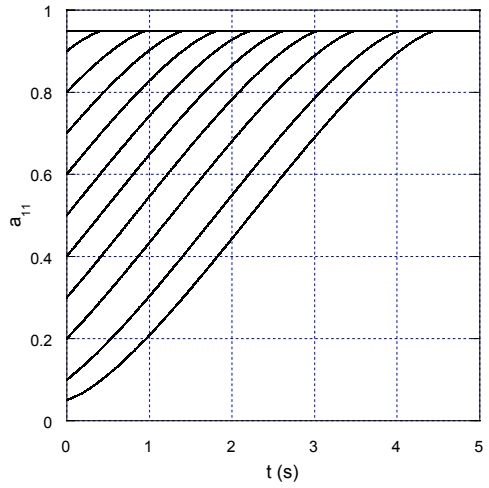

Fig. 7: time evolution of $\underline{\underline{\mathbf{a}}}$ (a_{11}) for various initial fibre orientation $\underline{\underline{\mathbf{a}}}_0$ ($a_{11}(t_0)$) – $f^{(f)} = 0.25$, $\lambda = 1$ s^{-1}.

Based on the results obtained in this work, it is then possible to compute the evolution of the macroscopic second order orientation tensor $\underline{\underline{\mathbf{a}}}$, integrating between an initial time t_0 and the current time t the following differential equation:

$$\dot{\underline{\underline{\mathbf{a}}}} = f\ (\ \underline{\underline{\mathbf{a}}},\ \underline{\underline{\mathbf{D}}},\ f^{(f)}\ ) \tag{5}$$

This is illustrated in fig.7, in the particular case where $f^{(f)} = \text{cst}$ and $\lambda = \text{cst}$ for various initial orientation $\underline{\underline{\mathbf{a}}}_0$. To obtain these curves, experimental data of fig. 4 ($\dot{a}_{11}$) were fitted using the following function (see the continuous line in fig.4):

$$\dot{a}_{11} = \alpha \left(1 - \frac{(\ a_{11} - 0.5\ )^2}{\beta^2} \right)^{\varphi} \tag{6}$$

where $\alpha = 0.25$, $\beta = 0.45$ and $\varphi = 0.3$.

5 CONCLUSION

Results gained here with the homogenisation of discrete structures bring useful information on the flow induced fibre orientation of highly concentrated fibre suspensions. Current developments focus on two aspects. On one hand, these results are used to propose a macroscopic model for fibre orientation. On the other hand, an extension of the present work to non-Newtonian fibre-fibre interaction is investigated.

REFERENCES

1. Petrich M.P., Koch D.L., *Phys. Fluids*, 10 (8) (1998) 2111-2113.
2. G.K. Batchelor, *J. Fluid Mech.*, 46 (4) (1971) 813-829.
3. Servais C., Månson J.-A. E., *J. Rheol.*, 43 (4) (1999) 991-1004.
4. Servais C., Luciani A., Månson J.-A. E., *J. Rheol.*, 43 (4) (1999) 1005-1018.
5. G. Moreau, D. Caillerie, *Computers and Structures*, 68 (1998) 181-189.
6. H. Tollenaere, D. Caillerie, "Continuous modeling of lattice structures by homogenization", *Adv. in Eng. Softwares,* 29 (7/9) (1998) 699-705.
7. Le Corre S., Caillerie D., Favier D., Orgéas L., In: *Proc. FRC 2000*, ed. A.G. Gibson, Woodhead Pub. Ltd, Newcastle/Tyne, U.K., 1 (2000) 303-310.
8. Le Corre S., Orgéas L., Favier D., Caillerie D., In: *Proc. 4th ESAFORM Conf.*, ed. A.M. Habraken, Liège, Belgium, 2 (2001) 453-456.
9. Le Corre S., *PhD. Thesis*, Univ. Joseph Fourier, Grenoble, France, (2001).
10. S. Toll, *J. Rheol.*, 37 (1) (1993) 123-125.
11. Yamane Y., Kaneda Y., Doi M., *J. Phys. Soc. Jpn*, 64 (9) (1995) 3265-3274.
12. Fan X., Phan-Thien N., Zheng R., *J. Non-Newtonian Fluid Mech.*, 74 (1998) 113-135.
13. Advani S. G., Tucker III C. L., *J. Rheol.*, 31 (8) (1987) 751-78